

Relevance of the catalytic activity on the performance of a NiO/CaAl₂O₄ oxygen carrier in a CLC process[☆]

A. Cabello, P. Gayán, F. García-Labiano*, L.F. de Diego, A. Abad, M.T. Izquierdo, J. Adámez

Instituto de Carboquímica (ICB-CSIC), Department of Energy and Environment, Miguel Luesma Castán 4, Zaragoza 50018, Spain

ARTICLE INFO

Article history:

Received 20 August 2013

Received in revised form 14 October 2013

Accepted 15 October 2013

Available online 24 October 2013

Keywords:

CO₂ capture

Chemical-looping combustion

Nickel

Oxygen carrier

Methane reforming

ABSTRACT

This paper presents a detailed investigation related to the physical and chemical changes underwent by a low Ni content oxygen carrier during 90 h of continuous operation in a CLC plant [1]. The oxygen carrier reached a combustion efficiency of 99% with a metallic Ni inventory of 17 kg/MW_{th}, which was the lowest value found in literature for any kind of Ni-based oxygen carrier. The present study was carried out in order to find the reasons by which this material exhibited a different combustion behavior in relation to other Ni-based oxygen carriers. Fresh and after-used particles were characterized by several techniques. XRD, TPR-TPO and XPS techniques proved that the use of CaAl₂O₄ as oxygen carrier support avoided the formation of NiAl₂O₄, which is a less reactive Ni-based compound than NiO and always formed in other Ni-based materials. The fact that all the NiO impregnated was found as free NiO in the oxygen carrier particles implied that this material maintained a high reactivity after 90 h of continuous CLC operation. The results obtained in the batch fluidized bed reactor have revealed the great relevance of the catalytic activity of the metallic Ni on the global fuel gas combustion process. The low Ni content present in this material makes necessary the use of very high reduction solid conversion to have enough metallic Ni in the fuel reactor to catalyze the CH₄ reforming reaction, and therefore to obtain high combustion efficiencies. This result will become very relevant for the design of a CLC unit using this Ni-based material as oxygen carrier.

© 2013 The Authors. Published by Elsevier B.V. All rights reserved.

1. Introduction

During last decade, several carbon capture and storage (CCS) technologies are being developed. Among them, chemical looping combustion (CLC) has the potential to make carbon capture significantly cheaper than current systems. CLC is a process in which the oxygen is transferred from air to the fuel by means of a solid oxygen carrier avoiding the direct contact between fuel and air. A key aspect for the successful development of CLC technologies is the selection and preparation of adequate oxygen carriers [2]. A suitable oxygen carrier for the CLC process must present some characteristics such as a high reaction rate with the fuel, complete fuel conversion to CO₂ and H₂O, sufficient oxygen transport capacity, high mechanical strength, low attrition rate, and good fluidization properties in order to avoid agglomeration problems. Furthermore, the selected material must be able to maintain these characteristics during as much number of redox cycles as possible.

During the last years, many efforts have been made to develop oxygen carriers suitable for the different CLC processes. Among the possible candidates, Ni-based oxygen carriers have been the most extensively used due to their high reactivity and good performance working with gaseous fuels [2].

The main disadvantages of using nickel oxide as oxygen carrier in an industrial CLC plant are the price and the environmental concerns. Both reasons could be lessened using particles with low nickel content but maintaining a high reactivity. Up to now, alumina has been widely used as support for Ni-based oxygen carriers. The use of this material as support improves some of the physical properties of the oxygen carrier such as the mechanical strength or the agglomeration behavior. However, reduction of NiO/Al₂O₃ particles is limited by the partial transformation of NiO into NiAl₂O₄ spinel compound [3,4], which has poor reactivity for CLC [5]. To avoid or to minimize the interaction of NiO with alumina, some modifications of the support via thermal treatment or chemical deactivation can be carried out in order to increase the reactivity of the Ni-based oxygen carrier. The addition of CaO or MgO to the NiO/Al₂O₃ mixture improves the behavior of the oxygen carrier by means of the formation of a spinel structure i.e. MgAl₂O₄ or CaAl₂O₄ [6].

Our research group at the Instituto de Carboquímica (ICB-CSIC) developed a very high reactive Ni-based oxygen carrier with a low

* This is an open-access article distributed under the terms of the Creative Commons Attribution License, which permits unrestricted use, distribution, and reproduction in any medium, provided the original author and source are credited.

Corresponding author. Tel.: +34 976 733 977; fax: +34 976 733 318.

E-mail address: glabiano@icb.csic.es (F. García-Labiano).

Table 1

Main characteristics of fresh and after-used particles of the Ni11CaAl material.

	Units	Fresh	After-used ^b
NiO content	(wt%) ^a	11.8	9.6
Oxygen transport capacity, R_{oc}	(%)	2.5	2.1
Particle density	(kg/m ³)	1400	1600
Crushing strength	(N)	1.2	0.6
Porosity	(%)	40.4	36.4
Specific surface area BET	(m ² /g)	2.1	2.4

^a Determined by TGA.^b 90 h in a 500 W_{th} CLC unit.

Ni content (11.8 wt% NiO) using CaAl₂O₄ as support, and avoiding the formation of the Ni spinel compound, NiAl₂O₄ [1]. This carrier was designated as Ni11CaAl. Combustion tests with different fuel gases i.e. CH₄, CO, H₂, syngas and light hydrocarbons (C₂H₆ and C₃H₈) were conducted in a 500 W_{th} continuous CLC unit. Using methane as fuel gas, a very high combustion efficiency was reached at oxygen carrier-to-fuel ratio (ϕ) values close to 1 (1.1–1.2). A further increase in the value of this parameter produced a decrease in the combustion efficiency. This behavior was different to that found using most of the Ni-based oxygen carriers present in the literature. Another remarkable result of this research work was that the solids inventory needed to obtain a methane combustion efficiency of 99% was 180 kg/MW_{th}, which corresponded to a metallic Ni inventory around 17 kg/MW_{th}, being this value the lowest referred in the literature for any other Ni-based oxygen carrier.

It must be also considered that the scale up of the CLC technology is a relevant issue that needs to be accomplished in the next years. A key point to achieve this objective is the development of appropriate CLC reactor engineering for each case. The understanding of the reaction mechanism between the oxygen carriers and the fuel plays a significant role in the determination of important design variables such as solid circulation rates or solids inventories.

In this work, a deep investigation related to the physical and chemical changes underwent by the Ni11CaAl particles during the continuous operation in the CLC pilot plant were carried out to find the reasons of the different behavior of this material in relation to other Ni-based oxygen carriers. For that, fresh and after-used particles of this oxygen carrier were characterized by several techniques and additional combustion tests were conducted in a batch fluidized bed reactor. This result will become very relevant for the design of a CLC unit using this Ni-based material as oxygen carrier.

2. Experimental

2.1. Oxygen carrier

A Ni-based oxygen carrier supported on CaAl₂O₄, so-called Ni11CaAl, was used in this work. The desired phase active loading (11.8 wt%) was obtained by applying two successive impregnation steps on a CaAl₂O₄ support. A detailed explanation of the preparation of this oxygen carrier can be found in the work of Gayán et al. [1].

The main properties of the fresh and used particles after 90 h of operation are presented in Table 1. The oxygen transport capacity was defined as the percentage of mass fraction of oxygen that could be used in the oxygen transfer, calculated as $R_{oc} = [(m_{ox} - m_{red})/m_{ox}] \times 100$, where m_{ox} and m_{red} were the masses of the oxidized and reduced form of the oxygen carrier respectively.

2.2. Oxygen carrier characterization techniques

Fresh and after-used particles of the oxygen carrier were physically and chemically characterized by several techniques.

The force needed to fracture a particle was determined using a Shimpo FGN-5X crushing strength apparatus. The crushing strength was taken as an average value of at least 20 measurements.

The porosity was measured by Hg intrusion in a Quantachrome PoreMaster 33, whereas the specific surface was determined by the Brunauer–Emmett–Teller (BET) method by adsorption/desorption of nitrogen at 77 K in a Micromeritics ASAP-2020 (Micromeritics Instruments Inc.).

The identification of crystalline chemical species was carried out by powder X-ray Diffraction (XRD) in a Bruker AXS D8 Advance, with Bragg–Brentano geometry configuration, Cu K α radiation and equipped with secondary graphite monochromator.

The microstructure of the particles was analyzed by means of a scanning electron microscope (SEM) ISI DS-130. This equipment was coupled to an ultra thin window PGT Prism detector for energy-dispersive X-ray (EDX) in order to carry out an elemental microanalysis.

The reducibility of the samples was determined by temperature-programmed reduction (TPR) experiments in a flow apparatus AUTOCHEM II from Micromeritics, equipped with a TCD detector. During these experiments, the accuracy in the measurements of the TPR peak was ± 1 K. The amounts of H₂ consumed were monitored continuously. About 250 mg of sample was placed in a quartz tube. Prior to the TPR experiment, the sample was flushed with Ar during 1 h. After this pretreatment, samples were heated at 7 K/min from room temperature to 1273 K with a flow of 20 ml/min of a mixture 10 vol% H₂/90 vol% Ar. Temperature programmed oxidation (TPO) runs were performed after cooling down the sample, using 20 ml/min of a mixture 5 vol% O₂/95 vol% He and heating up to 1273 K at 15 K/min. After TPO experiments, new TPR experiments were conducted at the same experimental conditions than the first ones.

Finally, X-ray photoelectron spectroscopy (XPS) results were recorded with an ESCAplus OMICRON system equipped with a hemispherical electron energy analyzer. The spectrometer was operated at 10 kV and 15 mA, using a non-monochromatized Mg K α X-ray Source ($h\nu = 1253.6$ eV) and under vacuum ($< 5 \times 10^{-9}$ Torr). Analyzer pass energy of 50 eV was used for survey scans and 20 eV for detailed scans. Binding energies (BE) were referenced to the C1s peak (284.5 eV) from adventitious carbonaceous contamination. A survey scan (1 sweep/200 ms dwell) was acquired between 1100 and 0 eV. Current region sweeps for Ni 2p, O 1s, C 1s, Al 2p and Ca 2p were obtained. The CASA data processing software allowed smoothing, Shirley type background subtraction, peak fitting and quantification. The amount of each element was calculated from intensity ratios using Scofield sensitivity factors [7].

2.3. Reactivity tests in TGA

Reactivity tests of fresh and after-used particles were carried out in a TGA, CI electronics type, described elsewhere [8]. The objective of these TGA tests was to evaluate if the oxygen carrier particles maintained the reactivity after long operation times. The reduction reactivity of the oxygen carrier was determined with CH₄, H₂, and CO. Pure air was used to study the oxidation reactivity of the material. The NiO content, and the corresponding oxygen transport capacity of the particles, were determined by thermogravimetric analysis using H₂ as reducing agent.

2.4. Batch fluidized bed tests

Reduction–oxidation multicycles were carried out to after-used oxygen carrier particles (90 h of operation) in a batch fluidized bed reactor to determine the gas product distribution obtained during the reaction of the Ni11CaAl material with CH₄ and air, respectively. The experimental set-up was described elsewhere [9]. The tests

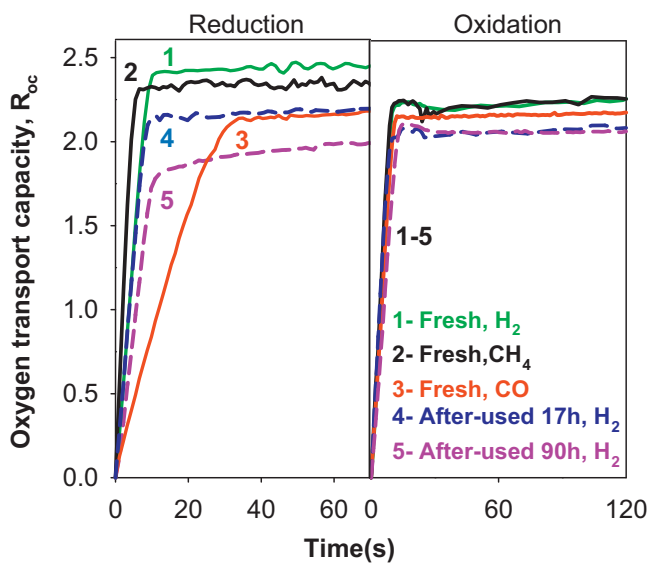


Fig. 1. Oxygen transport capacity vs time curves for reduction and oxidation reactions of fresh and after-used oxygen carrier particles using CH_4 , H_2 , CO as reacting gases for reduction, and air for oxidation. $T = 1223\text{ K}$. 3rd cycle.

were carried out at two different temperatures, 1103 and 1173 K, with an inlet superficial gas velocity into the reactor of 0.1 m/s. The composition of the reacting gas was 15 vol% CH_4 in N_2 during reduction and 10 vol% O_2 in N_2 during oxidation. The reduction periods were varied between 90 and 270 s. The oxidation periods needed for complete oxidation varied between 600 and 1200 s. To avoid the mixture of combustible gas with air, nitrogen was introduced during 120 s after each reducing and oxidizing period. The oxygen carrier was exposed to 35 reduction/oxidation cycles.

3. Results and discussion

Fresh and after-used particles of the Ni11CaAl material were characterized to determine the physical and chemical changes underwent by these particles during the 90 h of continuous operation carried out in the 500 W_{th} CLC pilot plant. The objective was to find the reasons of the different gas combustion behavior of this material with respect to other Ni-based oxygen carriers previously tested in continuous CLC prototypes.

3.1. Reactivity of the oxygen carrier

Fig. 1 shows the oxygen transport capacity, R_{oc} , vs time curves during reactivity tests in TGA with respect to several fuels (CH_4 , H_2 , CO) for fresh oxygen carrier and samples extracted at different operation times from the CLC plant. The oxygen carrier reactivity corresponding to the 3rd cycle was considered for comparison purposes. Fresh oxygen carrier particles exhibited a very fast reduction reaction with respect to H_2 and CH_4 , reaching a 90% of the total oxygen transport capacity in less than 10 s, being slower for CO . These results agreed with the ones obtained by Abad et al. [10], who found that an impregnated Ni-based oxygen carrier exhibited the highest reactivity working with H_2 and the lowest with CO . Nevertheless, the reactivity of the Ni11CaAl material was considerably improved with regard to other Ni-based oxygen carriers developed by dry impregnation using $\gamma\text{-Al}_2\text{O}_3$ as support for which reduction times higher than 300 s were needed to obtain a reduction conversion of 80% [6]. This important enhancement of the reduction reactivity could be explained by the use of CaAl_2O_4 as a support which allow that most of the NiO impregnated was present as free NiO in the oxygen carrier particles. In addition, both fresh and after-used

oxygen carrier particles presented high oxidation reactivity reaching values very close to 90% of the total oxygen transport capacity in less than 20 s.

The evolution of the oxygen transport capacity of the Ni11CaAl material was assessed throughout the time of operation in the CLC unit by means of additional TGA experiments. The active metal content of particles was determined from the TGA tests carried out with 15 vol% H_2 . The R_{oc} value of 2.5% obtained for the fresh particles was high enough to transfer the oxygen necessary to fully convert the fuel to CO_2 and H_2O [1]. Fig. 1 also illustrates the oxygen transport capacity of the particles after 17 h and 90 h of operation. As it can be observed, this parameter was reduced as the time of operation increased. In terms of active NiO content in the oxygen carrier particles, the value decreased from 11.8 wt% in the fresh particles to 9.6 wt% in the used particles after 90 h of continuous operation. Nevertheless, the reactivity of the used particles was maintained high after the whole experimental tests.

3.2. Mechanical strength and attrition rate

Mechanical strength is a parameter related with the lifetime of the particles. Fresh particles of the Ni11CaAl oxygen carrier presented a crushing strength of 1.2 N, and this value decreased up to 0.6 after 90 h of continuous operation at high temperature. Previous works in the literature reported that values under 1 N might be too soft to carry out, at optimum conditions, a long-term circulation process in fluidized beds [11].

In addition, the attrition rate measured during continuous operation in the CLC plant was high during the first hours of operation as a result of the rounding effect on the irregularities of the particles and the fines stuck to the particles during preparation. This parameter was stabilized after 40 h of operation at 0.25 wt%/h approximately, which meant a particle lifetime of 400 h. This particle lifetime value is quite low in comparison with other Ni-based oxygen carriers previously used [12,13]. The reason for so high attrition rate was related with the method of support preparation. It must be considered that the CaAl_2O_4 used as support was prepared at lab-scale by a method consisted on pelletizing a mixture of $\gamma\text{-Al}_2\text{O}_3$, CaCO_3 and graphite, followed by calcination at high temperature and milling. However, it is believed that better results would be obtained using commercial supports or manufactured at industrial scale.

The NiO content in the fine particles recovered in cyclones and filters was significantly higher than that in fresh oxygen carrier particles due to the abrasive attrition of the particles. In this sense, it must be considered that fresh particles had the external surface covered by small grains of NiO which could be separated from the support by attrition and elutriated during operation. This phenomenon brought about a decrease of the oxygen transport capacity, as it was previously mentioned.

3.3. SEM-EDX characterization

Some oxygen carrier particles were analyzed by SEM to determine possible changes produced in their internal structure during operation. Fig. 2 illustrates SEM images of fresh and after-used particles. Fresh oxygen carrier particles exhibited the usual irregular shapes of the support. The used particles presented a rounded shape as a consequence of the operation in the CLC plant. Some particles were embedded in resin epoxy, cut, and polished to analyze their internal structure. Images of cross sections of fresh and after-used particles were shown in Fig. 2b. No substantial changes in the internal structure were observed. In this sense, fresh and after-used particles exhibited a high porosity with large pores of 20–40 μm interconnected among them. The EDX analyses confirmed that the nickel content was distributed homogeneously with no

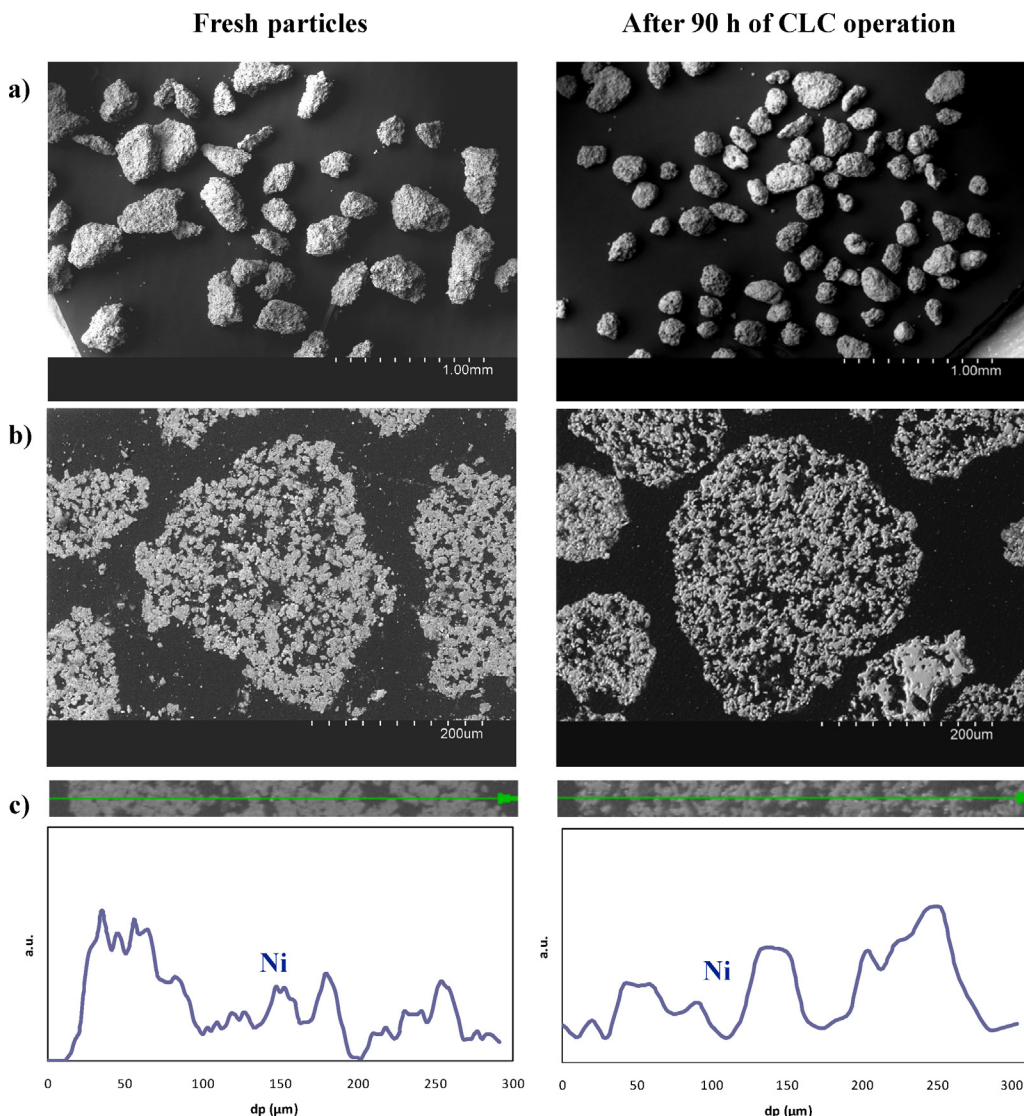


Fig. 2. SEM-EDX images of the oxygen carrier particles of both fresh and after 90 h of operation in the CLC unit: (a) SE (secondary electrons) image of the particles; (b) BSE (back-scattering electrons) image of a cross section of a particle; (c) EDX line profile of Ni in a cross section of a particle.

redistribution or migration of the metal oxide along the cyclic operation in the CLC plant (see Fig. 2c).

Finally, it is important to highlight that no signs of agglomeration were observed in the SEM images. This result agreed with the absence of defluidization problems obtained in the CLC unit during combustion operation.

3.4. XRD analyses

XRD analysis showed that the unique Ni-based crystalline phase present in fresh particles of the Ni₁₁CaAl oxygen carrier was NiO. The strong interaction of the Ca with Al₂O₃ to generate two calcium aluminates, CaAl₂O₄ and CaAl₄O₇, avoids the formation of NiAl₂O₄ in this material. This behavior was also observed in the particles extracted from the AR after 90 h of continuous operation. In the samples taken out from the FR of the CLC plant, Ni⁰ and NiO were the unique Ni-based crystalline phases detected.

3.5. Batch fluidized bed results

The usual behavior of any oxygen carrier operating in a continuous CLC plant includes an increase in the combustion efficiency

as higher is the oxygen carrier-to-fuel ratio used. However, the Ni₁₁CaAl exhibited a different behavior during the operation in the CLC plant [1]. The maximum combustion efficiencies, with values near 99%, were obtained at low oxygen carrier-to-fuel ratios ($\phi = 1.1\text{--}1.2$). Lower or higher values of ϕ produced a sharp decrease in the combustion efficiency. At $\phi < 1$, partial oxidation of fuel took place producing CO and H₂, however CH₄ did not appear at the FR outlet stream. At $\phi > 1.2$, CH₄ was the only unburnt product, indicating that the CH₄ partial oxidation/reforming reactions were not occurring at considerable amount in those conditions. Those facts indicated that fuel reaction occurred by different pathways depending on the ϕ value.

It must be considered that, in a continuous CLC process, the ϕ value is related to the variation of the solid conversion in the reactor, ΔX_S , and the reduction conversion of the oxygen carrier in the FR, X_r , as follows:

$$\Delta X_S = X_r = \frac{\eta_c}{\phi} \quad (1)$$

The combustion efficiency, η_c , can be defined as the ratio of oxygen consumed by the gas leaving the FR to that consumed by the gas when the fuel is completely burnt to CO₂ and H₂O. Furthermore,

Table 2
Reactions of Ni-based materials in the FR and AR.

Fuel reactor	
Combustion	$\text{CH}_4 + 4\text{NiO} \leftrightarrow 4\text{Ni} + \text{CO}_2 + 2\text{H}_2\text{O}$ (3)
	$\text{H}_2 + \text{NiO} \leftrightarrow \text{Ni} + \text{H}_2\text{O}$ (4)
	$\text{CO} + \text{NiO} \leftrightarrow \text{Ni} + \text{CO}_2$ (5)
Partial oxidation	$\text{CH}_4 + \text{NiO} \leftrightarrow \text{Ni} + \text{CO} + 2\text{H}_2$ (6)
Catalytic reforming	$\text{CH}_4 + \text{H}_2\text{O} \leftrightarrow \text{CO} + 3\text{H}_2$ (7)
	$\text{CH}_4 + \text{CO}_2 \leftrightarrow 2\text{CO} + 2\text{H}_2$ (8)
Water gas shift	$\text{CO} + \text{H}_2\text{O} \leftrightarrow \text{CO}_2 + \text{H}_2$ (9)
Methanation	$\text{CO} + 3\text{H}_2 \leftrightarrow \text{CH}_4 + \text{H}_2$ (10)
Coke formation	$\text{CH}_4 \leftrightarrow \text{C} + 2\text{H}_2$ (11)
	$\text{CO} + \text{H}_2 \leftrightarrow \text{C} + \text{H}_2\text{O}$ (12)
Carbon gasification	$\text{C} + \text{CO}_2 \leftrightarrow 2\text{CO}$ (13)
Air reactor	
Oxygen carrier oxidation	$\text{Ni} + \frac{1}{2}\text{O}_2 \leftrightarrow \text{NiO}$ (14)
Carbon combustion	$\text{C} + \text{O}_2 \leftrightarrow \text{CO}_2$ (15)
	$\text{C} + \frac{1}{2}\text{O}_2 \leftrightarrow \text{CO}$ (16)

the parameter ϕ was defined by Eq. (2), where F_{MeO} is the molar flow rate of the metal oxide, F_{Fuel} is the inlet molar flow rate of the fuel in the FR, and b is the stoichiometric coefficient of the fuel gas. A value of $\phi = 1$ corresponds to the stoichiometric MeO amount needed for maximum conversion of fuel to CO_2 and H_2O .

$$\phi = \frac{F_{\text{MeO}}}{b \cdot F_{\text{Fuel}}} \quad (2)$$

In this section, different combustion tests using CH_4 as fuel were carried out in a batch fluidized bed reactor with the objective of determining the reasons of the behavior of the Ni11CaAl material during CLC operation. For that, the possible reactions of the Ni-based materials inside the fuel and air reactors must be considered, which are shown in Table 2.

Fig. 3 illustrates the gas product distribution and the solid conversion obtained for the Ni11CaAl material working at 1173 K with a reduction period of 270 s and using CH_4 as reducing agent. The sample analyzed in the batch fluidized bed reactor corresponded to a used sample extracted from the CLC unit at the end of the experimental tests (90 h of operation) carried out by Gayán et al. [1]. During the first moments of reducing reaction, the CH_4 concentration was high. This situation in the batch fluidized bed reactor would be equivalent to the one present at the continuous CLC experimental set-up at which, for a high oxygen carrier-to-fuel ratio (ϕ) value, the resultant combustion efficiency (η_c) was low. The amount of unburnt CH_4 is high at these conditions because the amount of metallic Ni coming from the reduction of NiO is not enough to catalyze the CH_4 reforming reaction (Eq. (7)). The

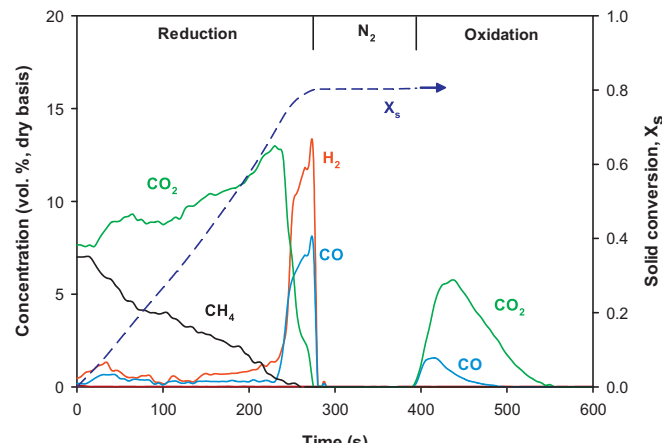


Fig. 3. Gas product distribution (dry basis) during a cycle in the batch fluidized bed reactor working with the Ni11CaAl material. Test conditions: $T = 1173\text{ K}$, 15 vol% CH_4 , reduction period = 270 s.

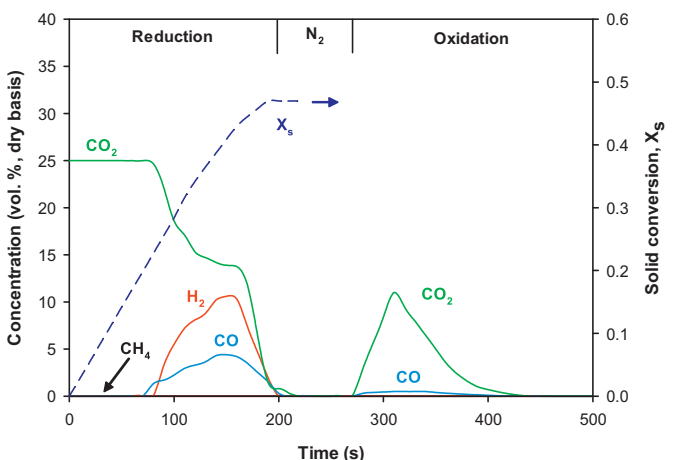


Fig. 4. Gas product distribution (dry basis) during a cycle in the batch fluidized bed reactor working with the Ni18- α Al:HI material. Test conditions: $T = 1173\text{ K}$, 30 vol% CH_4 , reduction period = 200 s.

unreacted amount of CH_4 decreased as the time was increased, i.e., as the reduction conversion of the oxygen carrier inside the batch fluidized bed reactor increased, and the catalytic activity of the Ni11CaAl material improved. In this sense, Pröll et al. [14] formulated a mechanism for the reaction between a Ni-based oxygen carrier and hydrocarbon fuels whose first step was based on the hydrocarbon conversion by the steam reforming reaction which was catalyzed by metallic Ni sites. When the solid reached conversion values about 0.7, the CO_2 concentration fell dramatically as a consequence of the oxygen depletion, and CO and H_2 concentrations started to increase. This period corresponds to ϕ values under 1 in the operation in the continuous unit. During the oxidation period, CO_2 and CO were generated by the combustion of C formed in the reduction period by coke formation reactions (Eqs. (11) and (12)).

As it was mentioned before, the Ni11CaAl presented a different combustion behavior in comparison with most of the previous Ni-based oxygen carrier materials tested in the literature [2]. For comparison reasons, Fig. 4 shows the gas product gas distribution obtained for the Ni18- α Al:HI material when CH_4 was used as reducing agent [15]. This oxygen carrier was developed in a previous work by dry impregnation over α -alumina [6] and widely tested in continuous CLC plants [13,16–18]. This material exhibited the usual behavior of the oxygen carriers in a CLC plant in such a way that an increase in the ϕ value produced an increase in the combustion efficiency. It can be observed that the highest CO_2 concentration was obtained immediately just after CH_4 feeding, which indicates that the fuel conversion was complete and mainly selective to CO_2 when the reduction conversion of the oxygen carrier, X_s , was low. Furthermore, CH_4 was not detected during the whole reduction period. CO and H_2 concentrations were negligible during the first part of the reduction period. The CO_2 concentration began to decrease and CO and H_2 appeared when the amount of oxygen available to convert the CH_4 was considerably reduced.

The difference behavior observed in both materials has two main reasons. By one hand, the formation of NiAl_2O_4 in the Ni18- α Al:HI catalyzes the reforming reaction allowing full methane combustion even at low solid conversion values [19]. On the other hand, the low Ni content present in the Ni11CaAl material and the no formation of NiAl_2O_4 makes necessary a very high reduction solid conversion to have enough metallic Ni to catalyze the CH_4 reforming reaction. This result agrees with that concluded by Ortiz et al. [19] who found that the catalytic activity of the oxygen carriers depended on their reduction/oxidation degree and that the

Table 3

Ni11CaAl samples subjected to TPR-TPO and XRD analyses.

Sample ^a	ϕ	ΔX_S	η_c (%)	XRD species
Fresh	—	—	—	NiO, CaAl ₂ O ₄ , CaAl ₄ O ₇
M3-AR	1.1	0.9	99	NiO, CaAl ₂ O ₄ , CaAl ₄ O ₇
M3-FR	1.1	0.9	99	Ni, NiO, CaAl ₂ O ₄ , CaAl ₄ O ₇
M7-AR	2.2	0.3	67	NiO, CaAl ₂ O ₄ , CaAl ₄ O ₇
M7-FR	2.2	0.3	67	Ni, NiO, CaAl ₂ O ₄ , CaAl ₄ O ₇

^a Samples references from Gayán et al. [1].

reforming reactions are of great relevance to achieve a complete CH₄ conversion when using Ni-based materials.

3.6. Temperature-programmed analyses

Temperature programmed reduction-oxidation (TPR-TPO) analyses were carried out to fresh and after-used particles of the Ni11CaAl oxygen carrier to analyze the reduction reactivity of this material and, specifically, the possible variation in the interaction degree between the active metal oxide, NiO, and the support, CaAl₂O₄.

Five different samples were subjected to TPR-TPO tests: a fresh sample of the Ni11CaAl oxygen carrier and samples extracted both from FR and AR after M3 and M7 tests carried out by Gayán et al. [1] using methane as fuel gas (see Table 3). The highest combustion efficiency was achieved during the M3 test. During this test, the oxygen carrier particles exhibited a high reduction conversion of the active metal oxide, NiO ($\Delta X_S \sim 0.9$). The conditions at the M7 test were completely different: the oxygen carrier-to-fuel ratio was high (2.2), which meant a low reduction conversion of NiO ($\Delta X_S \sim 0.3$) and, consequently, a low CH₄ combustion efficiency value. Table 3 shows the XRD species determined for the samples.

Bulk NiO and CaAlO support (mixture of 25% CaAl₂O₄ and 75% CaAl₄O₇, according to XRD) were used as reference materials for TPR tests. For bulk NiO powder, the TPR curve showed a single peak of hydrogen consumption with a maximum at 604 K. For CaAlO support an almost negligible shoulder of hydrogen consumption was observed at 593 K.

Fig. 5 illustrates TPR-1 and TPR-2 profiles for the different samples. TPR-2 profiles corresponded to TPR experiments conducted after oxidation of the samples in a TPO experiment. Table 4 shows the position of all the peaks from TPR-1 profiles and the NiO reducible calculated from these analyses. Fresh sample exhibited two shoulders at 673 K and 723 K and two peaks at 848 K and 973 K. First and second shoulders could be attributed to isolated NiO units on the surface of the support, probably with different crystal size. Peak at 848 K could be attributed to bidimensional NiO monolayer. Finally, the peak at 973 K could be attributed to a moderate interaction with the support forming amorphous Ni-Ca-Al. Nevertheless, the presence of the possible phase NiAl₂O₄ was not detected as it was also concluded from the XRD analyses. The peak corresponding to NiAl₂O₄ would be detected at 1143 K as it was obtained for the Ni18- α -Al:HI material [20], a Ni-based oxygen carrier impregnated on α -Al₂O₃. This TPR data confirm that the use of CaAl₂O₄ as

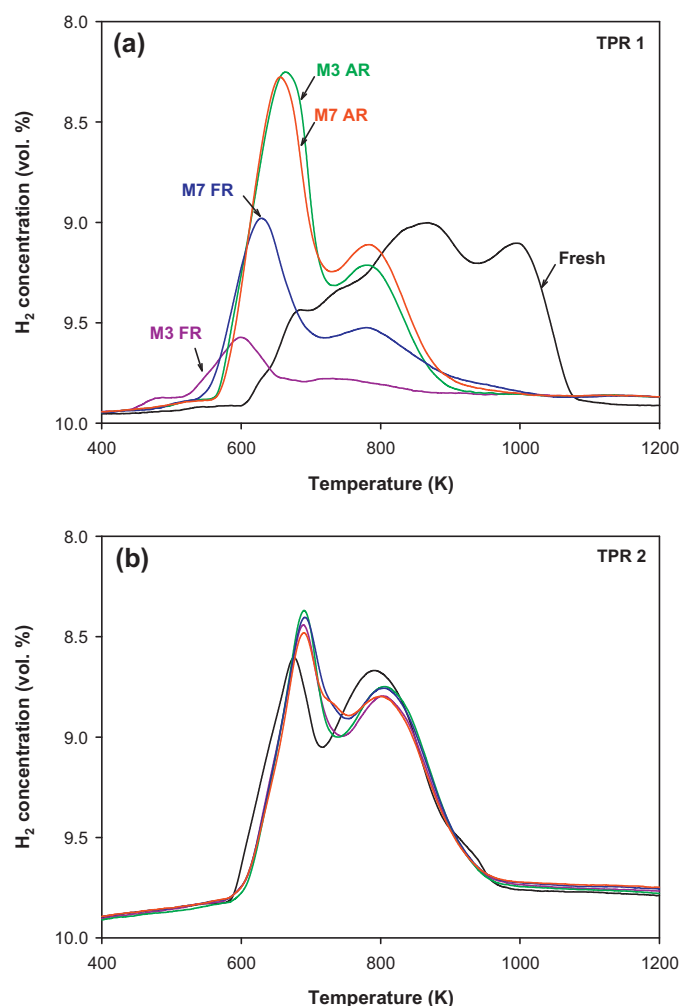


Fig. 5. TPR profiles of Ni11CaAl oxygen carrier particles, fresh and used.

support avoids the formation of NiAl₂O₄, maintaining the high reactivity of the free NiO and the good behavior demonstrated during operation in the CLC plant.

TPR-1 of the samples extracted from the AR gave two peaks at ~ 650 K and ~ 760 K. Comparing the first peak of the M3-AR and M7-AR samples with the one obtained in the fresh sample, it could be concluded that the crystallite size from the formers were homogenized since the resulting peaks were well defined and they did not present any shoulder. First peak could be attributed to isolated NiO units on the surface of the support. The second peak could be attributed to bidimensional NiO monolayer on the top of the support and it could be said that the interaction with the support was weak for both samples.

Regarding the samples extracted from the FR, TPR-1 profile of sample M3-FR exhibited a peak at 583 K and a shoulder at 713 K. The first peak could be attributed to bulk NiO and the shoulder to different interaction ranging from NiO isolated on the support and bidimensional NiO monolayer. In this case, the amount of NiO present in the sample was low as it was expected since the reduction conversion degree of the NiO inside the oxygen carrier particles was quite high ($\Delta X_S \sim 0.9$) as it was mentioned before (see Table 4). Furthermore, from the TPR-1 profile it could be also affirmed that the interaction of NiO with the support was weak. In addition, the TPR-1 profile of sample M7-FR presented two peaks of H₂ consumption at 623 K and 758 K, respectively. The first peak could be attributed to bulk NiO, but it was shifted to a higher temperature. This was probably due to the fact that this sample contained a

Table 4

Position of peaks and NiO contents (wt%) calculated from TPR-1 profiles. Data in K.

Sample	TPR-1	NiO content (wt%) obtained from TPR-1
Fresh	673 ^a , 723 ^a , 848, 973	11.3
M3-FR	583, 713 ^a	3.2
M3-AR	653, 760	9.9
M7-FR	623, 758	6.6
M7-AR	648, 763	10.7

^a Shoulder.

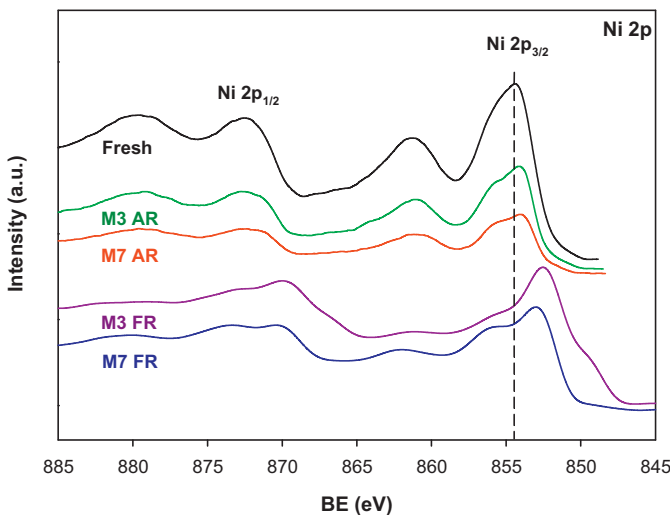


Fig. 6. XPS surface spectra for Ni 2p of Ni11CaAl oxygen carrier particles, fresh and used.

higher amount of NiO since the reduction conversion degree of NiO was quite lower ($\Delta X_S \sim 0.3$). The second peak could be attributed again to bidimensional NiO monolayer. In conclusion, the profiles of both samples taken from the FR were similar, but the amount of NiO interacting with the support is higher for the sample M7-FR since this sample contained a higher amount of NiO. Finally, it is important to highlight that the NiAl₂O₄ phase was not detected in any of the after-used samples analyzed, neither from the FR nor from the AR. This fact indicated that the Ca present in the support of the oxygen carrier particles was never substituted by elemental Ni. After oxidation of the samples in TPO experiments, new TPR profiles, TPR-2, were obtained. According to Fig. 5b, the profiles of the five samples were quite similar among them, indicating that after total oxidation of metallic Ni, the NiO-support interaction was almost identical. Due to the relatively weak interaction between NiO and the support, it can be concluded that nickel could not be dispersed as uniformly as desired in the oxygen carrier particles.

3.7. X-ray photoelectron spectroscopy (XPS) analyses

The same above samples were analyzed by XPS to characterize the surface of the Ni11CaAl oxygen carrier particles. This allowed us to identify the elements, the oxidation states and the type of chemical structure, as well as to quantify the mass percentage of each element.

Binding energy (BE) regimes containing the Ni 2p_{3/2} and Ni 2p_{1/2} emission lines of the Ni11CaAl samples were presented in Fig. 6. The position of the Ni 2p_{3/2} line for samples varied from 853.2 to 856.1 eV. For these samples, the position of the Ni 2p_{1/2} line was found at 17.6–18.4 eV higher BEs as compared to Ni 2p_{3/2} line, indicating the presence of Ni⁰ and Ni²⁺ in some samples. For both emission lines a shake up satellite was found at about 6.2–6.0 eV higher BEs from each emission line. The Ni 2p_{3/2} line around 856 eV with the associated satellite indicated the presence of one or more nickel-oxygen species. In the samples extracted from the FR, M3-FR and M7-FR, the peaks were shifted to lower BEs, indicating the presence of Ni⁰, and the shake-up shrank in both samples, in more extent for sample M3-FR. This fact was consistent with TPR results because the NiO present in M3-FR sample was more reduced than in sample M7-FR. BEs for samples extracted from the AR, M3-AR and M7-AR, were between pure NiO and NiAl₂O₄. However, from TPR and XRD analyses it was previously concluded that this later phase was never formed. The shift to higher BE would correspond to a stronger interaction than the one related to Ni²⁺ in octahedral

Table 5
Surface analysis from XPS spectra. wt% Ni for each peak is included in brackets.

Sample	Total Ni (wt.%)	Ni 2p region BE (eV)	
Fresh	9.97	854.1 (6.45)	856.1 (3.52)
M3-FR	3.14	853.6 (2.82)	855.3 (0.32)
M3-AR	6.25	854.0 (4.01)	856.1 (2.24)
M7-FR	2.59	853.2 (0.84)	855.2 (1.75)
M7-AR	4.55	854.0 (3.08)	856.0 (1.47)

sites of the supported Ni structure as NiO with weak interaction with the support.

The fitting of the peaks showed the presence of various contributions with BEs that were given in Table 5. As an example, Fig. 7 illustrates the fitting of the peaks obtained for the M3-AR sample. The BEs of the peaks were assigned to different Ni compounds according to data taken from literature [21,22].

Fresh sample exhibited two contributions: the first peak could be attributed to Ni²⁺ in octahedral sites of the supported Ni structure as bulk NiO and the second peak could be assigned to NiO with strong interaction with the support, but at BEs lower than that corresponding to NiAl₂O₄. However, no data concerning the interaction of NiO with the support (mixture of 25% CaAl₂O₄ and 75% CaAl₄O₇, according to XRD analysis) was found in the literature. So that, the Ca 2p region of the spectra for the five samples and the support were examined. In the case of the support, a peak corresponding to Ca 2p_{3/2} appeared at a BE of 346.9 eV, a higher value than the corresponding one to CaO, indicating the strong interaction between CaO and Al₂O₃, forming spinel structures, as it was shown by XRD. The BE for Ca 2p region for the five different samples did not change, indicating that there was not an interchange of Ca by Ni. In this sense, the strong interaction of NiO with the support could be due to the presence of bi-dimensional NiO monolayer in the top of the support.

Samples extracted from the AR exhibited quite similar spectra in relation to the fresh sample. The only difference was the change in the areas of each fitted peak which corresponded to different mass percentages of Ni (reported in Table 5). For both samples, the mass percentage of Ni calculated for each peak was lower than the one corresponding to the fresh sample.

The Ni 2p_{3/2} line for samples coming from the FR was shifted to lower BEs values, indicating the presence of metallic nickel. Moreover, it could be observed a shrunk of the shake-up satellite for both samples, especially for sample M3 FR, which contained a higher amount of Ni⁰ due to the higher reduction conversion degree of the

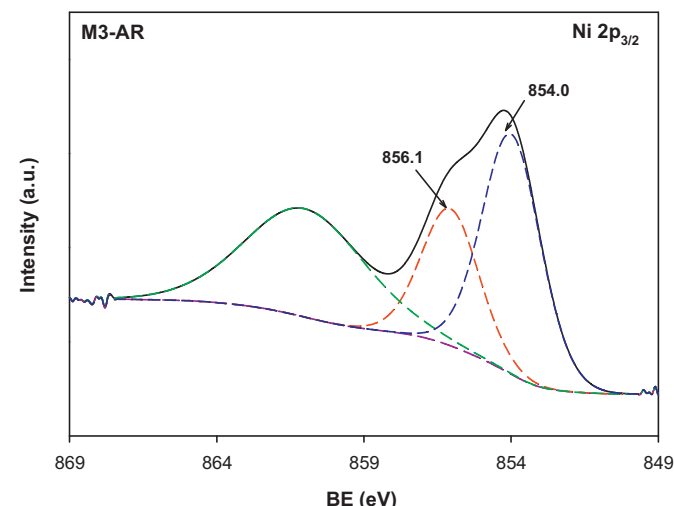


Fig. 7. Deconvolution of the XPS peaks of M3-AR sample in the Ni 2p_{3/2} region.

NiO present in the oxygen carrier particles in that test. The curve fitting of this line gave two peaks. The first peak corresponded to metallic Ni and the second peak to NiO with weak interaction with the support. The total amount of Ni present on the surface of these samples was similar, however the Ni distribution into components was quite different (see Table 5). For sample M3-FR, most of the Ni was present as metallic Ni due to its higher reduction conversion degree ($\Delta X_S \sim 0.9$) in comparison with the M7-FR test ($\Delta X_S \sim 0.3$). However, for sample M7-FR, most of the Ni was present as NiO with weak interaction with the support. Another difference between the samples extracted from FR after the corresponding experimental tests was the shift to lower BE of the peak corresponding to metallic Ni for sample M7-FR. This shift was most likely due to differentially charging [23]. This fact usually happens with large particles and with particles having no good electrical contact with the support.

As in the case of TPR-TPO tests, XPS analysis again demonstrated that the interaction of NiO with the support was not due to the formation of the less reactive Ni compound, NiAl_2O_4 , but due to the presence of bi-dimensional NiO monolayer in the top of the support.

Regarding the mass percentage of Ni present in the different samples analyzed and its distribution into components, it was confirmed the relation between the ϕ value used in the CLC tests and the metallic Ni content, which determines the catalytic activity of the Ni11CaAl material for CH_4 reforming reactions. Ortiz et al. [19] found that the catalytic activity of the impregnated Ni-based oxygen carriers for CH_4 reforming depended on their reduction degree, increasing the catalytic activity when the reduction conversion of the oxygen carrier was increased. Therefore, it could be said that the CH_4 reforming reactions were of great relevance to achieve a high CH_4 conversion in a CLC system. In the previous work carried out by Gayán et al. [1], since a low NiO content was used in the oxygen carrier, the relevance of the reduction degree needed to achieve full CH_4 conversion was more important. Only working at very low oxygen carrier-to-fuel ratios above stoichiometric conditions (1.0–1.2), which corresponded to high reduction conversion values ($\Delta X_S \sim 0.9$), almost full conversion of CH_4 was achieved due to the catalytic activity of the oxygen carrier in those conditions.

Two main reasons can be responsible for the low combustion efficiencies achieved with the Ni11CaAl material at $\phi > 1.2$ in the CLC plant. Firstly, the low reduction conversion degree of the oxygen carrier, ΔX_S , supposes that only a small fraction of the nickel present in the particles is in the form of metallic Ni, which is not enough to carry out the catalytic methane reforming reaction. Secondly, the low NiO content present in the particles, which is clearly beneficial from an environmental point of view, difficult the oxygen availability in the system for the CH_4 combustion through reactions (3)–(6).

Nevertheless, it was demonstrated that this is a highly reactive oxygen carrier, with a low NiO content, which can be used with high efficiency in a continuous CLC plant for combustion of gaseous fuels in a well-defined range of operating conditions. However, the CLC design would be influenced by the minimum solids inventory needed to fulfill the minimum metallic Ni requirements to produce the CH_4 reforming reaction in the FR.

4. Conclusions

A Ni-based oxygen carrier with a low NiO content (11.8 wt% NiO) previously used in a 500 W_{th} CLC unit [1] has been analyzed in terms of reactivity, gas product distribution, and characterization of physical and chemical properties after continuous operation.

Several characterization techniques, such as XRD, TPR-TPO, and XPS, have demonstrated that the use of CaAl_2O_4 as support avoided the formation of the low reactive Ni-based compound NiAl_2O_4 . This allowed that all the NiO impregnated was found as free NiO in the oxygen carrier particles giving it a high reactivity which was maintained during the 90 h of continuous operation in the CLC plant.

The results obtained in the batch fluidized bed reactor have revealed the necessity to use very high reduction solid conversion to have enough metallic Ni to catalyze the CH_4 reforming reaction, and therefore to obtain high combustion efficiencies. The no formation of NiAl_2O_4 and the low Ni content present in the Ni11CaAl material are the responsible of this behavior. These results have explained the high combustion efficiency values obtained with this material at low oxygen carrier-to-fuel ratios during the continuous tests carried out in the 500 W_{th} CLC unit.

Acknowledgements

This paper is based on the work performed in the frame of the INNOCUOUS (Innovative Oxygen Carriers Uplifting Chemical-Looping Combustion) Project, funded by the European Commission under the seventh Framework Program (Contract 241401).

References

- [1] P. Gayán, A. Cabello, F. García-Labiano, A. Abad, L.F. de Diego, J. Adámez, Int. J. Greenhouse Gas Control 14 (2013) 209–219.
- [2] J. Adámez, A. Abad, F. García-Labiano, P. Gayán, L.F. de Diego, Prog. Energy Combust. 38 (2012) 215–282.
- [3] R.J. Copeland, G. Alptekin, M. Cesario, Y. Gershmanovich, Proc. 1st National Conf. on Carbon Sequestration, NETL, Washington, DC, USA, 2001.
- [4] H.J. Ryu, N.Y. Lim, D.H. Bae, G.T. Jin Korean, J. Chem. Eng. 20 (2003) 157–162.
- [5] R. Villa, C. Cristiani, G. Groppi, L. Lietti, P. Forzatti, U. Cornaro, S. Rossini, J. Mol. Catal. A: Chem. 204–205 (2003) 637–646.
- [6] P. Gayán, L.F. de Diego, F. García-Labiano, J. Adámez, A. Abad, C. Dueso, Fuel 87 (2008) 2641–2650.
- [7] J.H. Scofield, J. Electron Spectrosc. Relat. Phenom. 8 (1976) 129–137.
- [8] J. Adámez, L.F. de Diego, F. García-Labiano, P. Gayán, A. Abad, Energy Fuels 18 (2004) 371–377.
- [9] L.F. de Diego, P. Gayán, F. García-Labiano, J. Celaya, A. Abad, J. Adámez, Energy Fuels 19 (2005) 1850–1856.
- [10] A. Abad, F. García-Labiano, L.F. de Diego, P. Gayán, J. Adámez, Energy Fuels 21 (2007) 1843–1853.
- [11] M. Johansson, T. Mattisson, A. Lyngfelt, Ind. Eng. Chem. Res. 43 (2004) 6978–6987.
- [12] A. Lyngfelt, B. Kronberger, J. Adámez, J.X. Morin, P. Hurst, E.S. Rubin, D.W. Keith, C.F. Gilboy, M. Wilson, T. Morris, J. Gale, K. Thambimuthu, Int. J. Greenhouse Gas Control 7 (2005) 115–123.
- [13] J. Adámez, C. Dueso, L.F. de Diego, F. García-Labiano, P. Gayán, A. Abad, Energy Fuels 23 (2009) 130–142.
- [14] T. Pröll, G. Schöny, K. Mayer, H. Hofbauer, Proc. 2nd Int. Conf. on Chemical Looping, Darmstadt, Germany, 2012.
- [15] C. Dueso, Doctoral Thesis, University of Saragossa, 2011.
- [16] F. García-Labiano, L.F. de Diego, P. Gayán, J. Adámez, A. Abad, C. Dueso, Ind. Eng. Chem. Res. 48 (2009) 2499–2508.
- [17] J. Adámez, C. Dueso, L.F. de Diego, F. García-Labiano, P. Gayán, A. Abad, Ind. Eng. Chem. Res. 48 (2009) 2509–2518.
- [18] C. Dueso, F. García-Labiano, J. Adámez, L.F. de Diego, P. Gayán, A. Abad, Fuel 88 (2009) 2357–2364.
- [19] M. Ortiz, L.F. de Diego, A. Abad, F. García-Labiano, P. Gayán, J. Adámez, Energy Fuels 26 (2012) 791–800.
- [20] C. Dueso, A. Abad, F. García-Labiano, L.F. de Diego, P. Gayán, J. Adámez, A. Lyngfelt, Fuel 89 (2010) 3399–3409.
- [21] C.D. Wagner, A.V. Naumkin, A. Kraut-Vass, J.W. Allison, C.J. Powell, J.R. Rumble, NIST (National Institute of Standards and Technology) X-ray Photoelectron Spectroscopy Database, 2003 <http://srdata.nist.gov/xps/>
- [22] C.D. Wagner, W.M. Riggs, L.E. Davis, J.F. Moulder, G.E. Mullenberg, Handbook of X-ray Photoelectron Spectroscopy, Perkin-Elmer Corp., Physical Electronics Div., Eden Prairie, MN, 1979.
- [23] M.A. Goula, A.A. Lemonidou, W. Grünert, M. Baerns, Catal. Today 32 (1996) 149–156.